

pubs.acs.org/JPCL Letter

Revealing the Structure and Noncovalent Interactions of Isolated Molecules by Laser-Desorption/Ionization-Loss Stimulated Raman Spectroscopy and Quantum Calculations

Afik Shachar,[§] Itai Kallos,[§] Mattanjah S. de Vries, and Ilana Bar*



Cite This: J. Phys. Chem. Lett. 2021, 12, 11273-11279

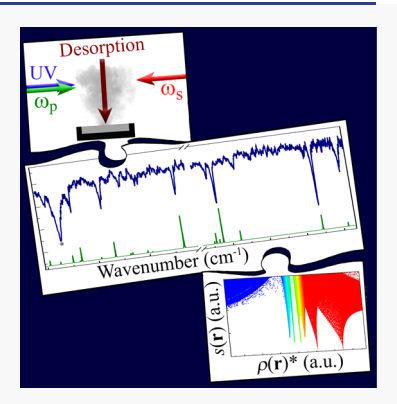


ACCESS

Metrics & More

Article Recommendations

ABSTRACT: The structural and dynamical characteristics of isolated molecules are essential, yet obtaining this information is difficult. We demonstrate laser-desorption jet-cooling/ionization-loss stimulated Raman spectroscopy to obtain Raman spectral signatures of nonvolatile molecules in the gas phase. The vibrational features of a test substance, the most abundant conformer of tryptamine, are compared and found to match those resulting from the scaled harmonic Raman spectrum obtained by density functional theory calculations. The vibrational signatures serve to identify the most prominent *gauche* conformer and evaluate its predicted electronic structure. These findings, together with noncovalent interaction (NCI) analysis, provide new insights into electron densities and reduced density gradients, assessing the hydrogen bonds (N–H··· π and C–H···H–C) and interplay between attractive and repulsive NCIs affecting the structure. This approach accesses vibrational signatures of isolated nonvolatile molecules by tabletop lasers at uniform resolution and in a broad frequency range, promising great benefit to future studies.



he development of a variety of spectroscopic techniques, combined with quantum molecular calculations, has made significant contributions to the study of structural and dynamical properties of biomolecules. 1-10 These methods include ion- and fluorescence-dip spectroscopies, with tunable microwave (MW), 11 infrared (IR), 12,13 visible (VIS), 14,15 and ultraviolet (UV)¹⁶ sources. In most cases, pump sources resonantly deplete the population of specific rovibrational states of ground-state molecules, subsequently probed by an additional laser beam, via action spectroscopy, involving laserinduced fluorescence¹⁷ and resonance-enhanced multi- or twophoton ionization (REMPI or R2PI). 18,19 This population depletion leads to reduced fluorescence or ion signals for excitations induced by the pump and probed from a shared level. The mass spectrometric (MS) detection of ion signals has the advantage of mass selectivity and is crucial for cluster studies. Moreover, the coupling with jet-cooling (JC) provides sufficient resolution for the separation of vibronic transitions of selected tautomeric, conformational, and structural isomers.

These double-resonant or hole-burning (HB) techniques probe vibronic or vibrational transitions of specific isomers, like conformers, tautomers, or cluster structures. Implementations include UV–UV HB,²⁰ infrared-ion-dip spectroscopy (IR-IDS),^{1–10} and ionization-loss stimulated Raman spectroscopy (ILSRS).^{15,21,24,25} In IR-IDS, it is possible to obtain IR signatures by scanning the IR "burn" wavelength while monitoring the R2PI ion signal from a "probe" UV laser, tuned to the transition of a specific isomer. Since IR lasers are

relatively limited in their wavelength range, most studies refer to the region covering the hydride stretch frequencies, while the assessment of far IR vibrational modes in 200–1800 cm⁻¹ range so far has been achieved only at a free-electron laser (FEL) facility¹ with lower resolution. Nowadays, there exists a limited possibility to overcome the challenge of monitoring vibrational signatures in the extended spectral range while using different sources, i.e., the far vibrational modes and the hydride stretch regions by FEL and an optical parametric oscillator, respectively.²⁶ Although this approach expands the excitation frequency ranges, it suffers from main drawbacks, i.e., FEL availability and limited spectral resolution.

Similar to IR-IDS, in ILSRS, ^{15,21–25} the UV laser is tuned to

Similar to IR-IDS, in ILSRS, $^{13,21-23}$ the UV laser is tuned to the transition of a specific isomer, but two different VIS beams, i.e., a fixed frequency pump (ω_p) and a tunable Stokes-shifted frequency (ω_S) are used, where $\omega_p - \omega_S$ can match Raman transitions of the probed species. Under these conditions, depletion of a certain percent of the ground vibrational-state population occurs, leading to a loss in the ionization signal and, consequently, to isomer-specific Raman signatures. In this approach, one uses VIS laser beams for promoting vibrationless

Received: October 10, 2021 Accepted: November 10, 2021



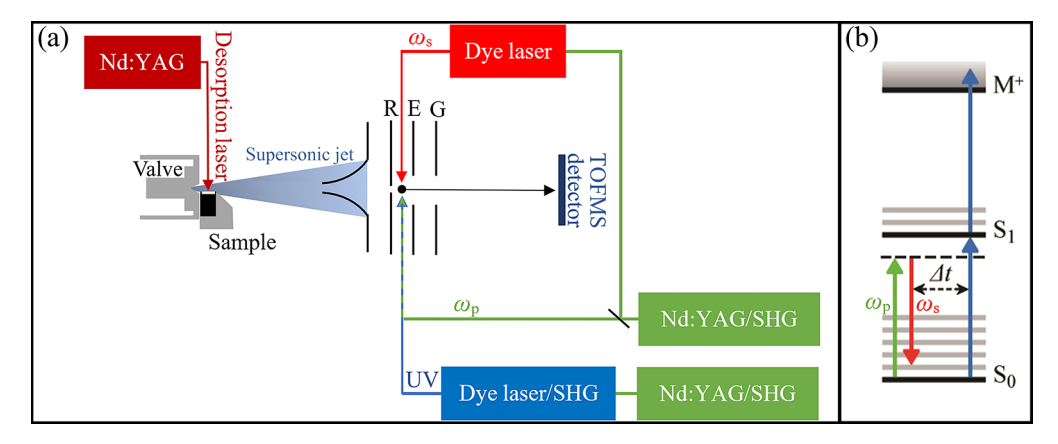


Figure 1. Schematic drawing of the (a) experimental system including the lasers with second-harmonic generators (SHGs) and the time-of-flight mass spectrometer (TOFMS) with repeller (R), extractor (E), and ground (G) electrodes; (b) the energy diagram presenting the ionization-loss stimulated Raman scattering processes.

ground-state isomers to fundamental, overtone, or combination vibrations, where the last two are considerably less intense and scarcely seen. Indeed, in our first attempt, SRS was induced, leading to features in the extended range of 900–3500 cm⁻¹ and later even in the 400–3650 cm⁻¹ range by using copropagating and counterpropagating VIS beams, respectively. The resulting ILSRS vibrational signatures in the extended spectral range highlight the importance of vibrations corresponding to collective motions and bends, positioned at low frequencies, rather than only hydride stretches for revealing skeletal structures and the intramolecular forces affecting their shape. In principle, ILSRS can cover the entire spectral region of the fundamental vibrations with a uniform resolution with the use of the proper tabletop lasers.

Up to now, a limitation of ILSRS of isolated molecules has been the demand for probing relatively volatile species. However, most biomolecules of interest are nonvolatile and might decompose upon heating, requiring specific vaporization techniques. One of the approaches for producing JC molecules and their clusters is laser desorption (LD)²⁷ combined with supersonic expansion.^{28–30} The LDJC technique involves the use of a pulsed laser to induce fast heating and to desorb molecules from a surface before they decompose. This approach has allowed the study of numerous flexible biological building blocks, consisting of backbones and side chains and existing as various conformers and isomers.^{1–8,10} Although the energy barrier between conformers or isomers is relatively low, LDJC allows isolating specific species.

The present study aims to demonstrate the feasibility of coupling a new compact and stable vaporization source for generating intact neutral molecules³¹ with ILSRS. Tryptamine (TRA), which contains a rigid indole moiety attached to a flexible ethylamino side chain, serves as an example of the conformer-specific spectroscopy made possible by this approach. Although this molecule has previously been vaporized by thermally heating the solid compound and studied by different spectroscopic methods,^{32–43} to identify its conformers, its structure and particularly the intramolecular noncovalent interactions (NCIs) are not fully understood, highlighting the necessity for obtaining this information. Here, a proof-of-concept study, in which a laser beam is delivered toward a pressed TRA/graphite mixture for LD into the gas phase and coupled with ILSRS, shows that the LD/ILSRS

combination for obtaining vibrational signatures is viable. In addition, comparison of the scaled harmonic spectrum of the dominant conformer, obtained by density functional theory (DFT) calculations, with the conformer-specific ILSR spectrum identified the most stable conformer of TRA and evaluated its predicted electronic structure. These findings provide insight into structural adjustments by NCI analysis ^{44,45} and help identify the interplay of attractive and repulsive interactions in this conformer.

We perform the experiments on a previously described system. 24,31 The schematic of Figure 1(a), LDJC coupled with ILSRS, Figure 1(b), shows the laser pulse sequence used to obtain the Raman signatures of the dominant conformer of TRA.

The spectrum of LDJC TRA, monitored by one-color R2PI in the $34\,810-34\,935$ cm⁻¹ range, ³¹ is essentially similar to that of heated JC TRA, ^{32,33,35,40,42} exhibiting unique bands, related to its different conformers. Considering that TRA consists of an indole moiety and a flexible ethylamino side chain with torsional degrees of freedom, about the C–N and two C–C single bonds, it is possible to obtain structures that mainly differ in the amino group position. In particular, the predominant conformer is the *gauche* conformer, denoted as Gpy(out), ³⁵ shown in Figure 2, where the amino hydrogen points toward the pyrrole π cloud, and the position of the nitrogen lone pair is away from the indole π cloud.

By tuning and parking the exciting UV laser beam on the most intense feature, positioned at 34 919 cm⁻¹³¹ and spatially overlapping it with the $\omega_{\rm p}$ and $\omega_{\rm S}$ beams, we measure the ILSR spectrum of the most stable conformer, obtained by LDIC of TRA while gating the molecular ion in the mass spectrometer (MS). We selected to monitor the ILSR spectrum of the Gpy(out) conformer in the low- (1300-1600 cm⁻¹) and highfrequency (3000-3450 cm⁻¹) ranges, shown in the upper trace of Figure 2. This spectrum displays an almost constant ion background level due to the R2PI signal of TRA, but at specific wavenumbers, sharp features of different intensities aiming downward emerge. Relying on the scheme of Figure 1(b), these features in the spectrum reflect the population depletion of the vibrationless ground state of the corresponding TRA conformer. Especially, for frequency differences $(\omega_p - \omega_s)$ matching resonant transitions to specific molecular vibrational modes, the ion signal drops, producing the ILSR spectrum, via scanning of ω_s . These features correspond to Q-branch

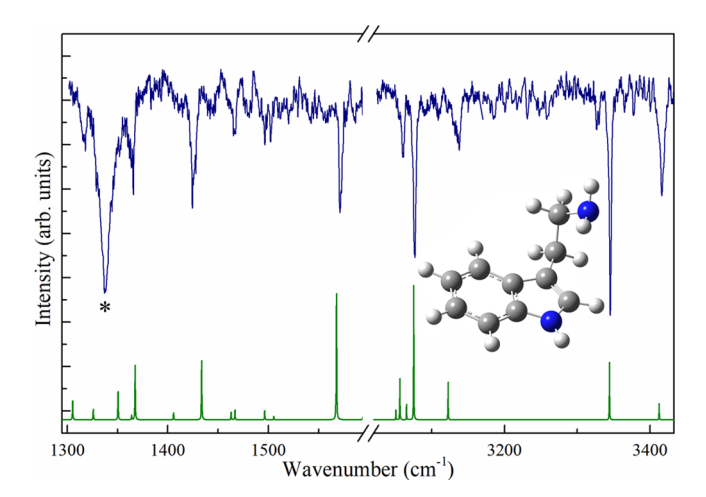


Figure 2. (a) The top trace displays the measured ionization-loss stimulated Raman (ILSR) spectrum of laser-desorbed jet-cooled tryptamine (TRA), probed at $34\,919~{\rm cm}^{-1}$, and the bottom trace is the computed spectrum, based on the derived Raman intensities convolved with Lorentzian lines (full width at half-maximum of 0.5 cm⁻¹) vs. the scaled harmonic vibrational frequencies at the B3LYP/6-311⁺⁺G(d,p) level of theory for the optimized geometry of the TRA GPy(out) conformer, shown in the central part.

rotational band contours for transitions to different vibrational modes, which occur by conservation of rotational states.

The calculated spectrum of the GPy(out) conformer of TRA is obtained by quantum chemical calculations at the B3LYP/6-311⁺⁺G(d,p) level of theory and is based on the optimized geometry of the structure shown in the central part of Figure 2. This spectrum, constructed from intensities deduced from Raman activities, 42 convolved with Lorentzian lines of full width at half-maximum (fwhm) of 0.5 cm $^{-1}$ and from scaled harmonic vibrational frequencies, is shown at the bottom of Figure 2. The calculated Raman spectrum of the TRA GPy(out) conformer agrees well with the measured ILSR spectrum, although not quantitatively.

By comparing the observed features to the calculated ones, it is possible to attribute them to different normal mode vibrations, where those corresponding to the dominant features in the ILRS spectrum of Figure 2 are portrayed in Figure 3. For instance, starting from the highest-frequency mode, the respective antisymmetric and symmetric N–H stretches of the ethylamino group and the symmetric C–H stretch mode of the benzene ring are shown in Figure 3(a–c). In the low-frequency range, modes corresponding to collective motions, mostly characterized by different high-amplitude movements of the atoms in the indole ring and some minor ones in the amino chain, are shown in Figure 3(d–f).

A unique feature, considerably broader than others, in the low-frequency range (1337 cm $^{-1}$) [marked with an asterisk (*)] appears in the ILSR measured spectrum, Figure 2. This feature is observed even upon blocking of the $\omega_{\rm p}$ beam, implying that it stems from a two-color VIS–VIS–UV–HB process, induced by $\omega_{\rm S}$. In this process, excitation with two VIS photons (17 460 cm $^{-1}$) burns a hole in the ion signal by resonantly depleting the TRA ground state.

The agreement between the calculated Raman and measured ILSR spectra confirms the identification of the TRA Gpy(out) conformer and its electronic structure. It is instructive to find out which interactions determine this structure. To extract and classify the intramolecular interactions that lead to the unique

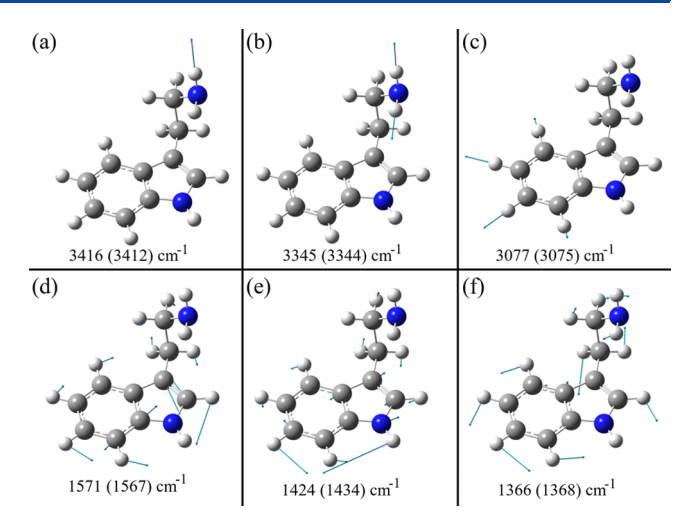


Figure 3. Geometry of the Gpy(out) conformer of tryptamine, following optimization at the B3LYP/6-311 $^{++}$ G(d,p) level of theory, together with the displacement vectors, generated with GaussView. The dominant features in the ILSR spectrum of Figure 2 correspond to various normal mode vibrations [(a–f)], where the measured and scaled harmonic (in parentheses) frequencies at the same level of theory are given at the bottom of each panel.

structure, we applied an NCI analysis. 44,45,47,48 This analysis utilizes a reduced density gradient, $s(\mathbf{r})$, given by

$$s(\mathbf{r}) = |\nabla \rho(\mathbf{r})|/2(3\pi^2)^{1/3}\rho(\mathbf{r})^{4/3}$$
(1)

where $\rho(\mathbf{r})$ represents the electron density and $|\nabla \rho(\mathbf{r})|$ represents its gradient, and the second eigenvalue of the electron-density Hessian (second derivative) matrix is represented by λ_2 . Regions with low $s(\mathbf{r})$ correspond to NCIs,⁴⁷ and those with a negative or positive sign of λ_2 are related to regions of locally increased or depleted electron density, referring to attractive or repulsive NCIs, respectively. Visualization plots of $s(\mathbf{r})$ vs. $\rho(\mathbf{r})^*$, corresponding to the product of the sign of λ_2 and the density $[= \text{sign}(\lambda_2)\rho(\mathbf{r})]$, should exhibit an exponential behavior in the absence of NCIs and an appearance of troughs in $s(\mathbf{r})$ in their presence. Furthermore, by plotting low-valued isosurfaces, it should be possible to visually examine the low- $s(\mathbf{r})$ regions and obtain information on the atoms involved in the NCIs.

Performing this NCI analysis, we identified and classified regions with low $s(\mathbf{r})$ values in the TRA Gpy(out) conformer, presented in Table 1 and Figure 4. By choosing a red, green, and blue (RGB) color scheme, we obtain the isosurfaces in Figure 4(a) and the visualization plot of $s(\mathbf{r})$ vs. $\rho(\mathbf{r})^*$ in Figure 4(b). The observed color variations in the isosurfaces, visualization plot, and the bottom arrows classify the interactions, whereas attractive (stabilizing) interactions appear in blue, repulsive (destabilizing) interactions appear in red, and delocalized weak interactions appear in green. As the darkness of the blue and red colors increases, the local densities of electrons are more affected, implying correspondingly stronger interactions.

Examination of the isosurfaces with $s(\mathbf{r})=0.6$ a.u., Figure 4(a), and of the visualization plot, Figure 4(b), suggests the presence of the interactions listed in Table 1. In particular, the N1–H14··· π [$\rho(\mathbf{r})^*=-0.0083$ a.u.], C11–H24···H17–C3 [$\rho(\mathbf{r})^*=-0.0037$ a.u.], and C2–H15···H24–C11 [$\rho(\mathbf{r})^*=-0.0035$ a.u.] interactions, denoted as A_i – A_{iii} , correspond to regions with $\lambda_2 < 0$, showing the occurrence of weak attractive

Table 1. Noncovalent Interactions in the Tryptamine Gpy(out) Conformer, Determined by the Noncovalent Interaction (NCI) Analysis^a

noncovalent interaction $\rho(\mathbf{r})^*$ (a.u.) $s(\mathbf{r})$ (a.u.) A_i N1-H14···π -0.0083 0.2018 A_{ii} C11-H24···H17-C3 -0.0037 0.4259 A_{iii} C2-H15···H24-C11 -0.0035 0.1512 RC _i C4-C5-N6-C7-C12 0.0493 0.0257 RC _{ii} C7-C8-C9-C10-C11-C12 0.0212 0.0828 RC _{iii} C4-C3-C2-N1-H14 0.0084 0.2024 RC _{ii} H17-C3-C4-C12-C11-H24 0.0041 0.4058 RC H15-C2-C3-C4-C12-C11-H24 0.0035 0.1612				
$\begin{array}{cccccccccccccccccccccccccccccccccccc$		noncovalent interaction	$\rho(\mathbf{r})^*$ (a.u.)	s(r) (a.u.)
$\begin{array}{cccccccccccccccccccccccccccccccccccc$	\mathbf{A}_{i}	N1-H14···π	-0.0083	0.2018
RC_i $C4-C5-N6-C7-C12$ 0.0493 0.0257 RC_{ii} $C7-C8-C9-C10-C11-C12$ 0.0212 0.0828 RC_{iii} $C4-C3-C2-N1-H14$ 0.0084 0.2024 RC_{iv} $H17-C3-C4-C12-C11-H24$ 0.0041 0.4058	A_{ii}	C11-H24···H17-C3	-0.0037	0.4259
RC _{ii} C7-C8-C9-C10-C11-C12 0.0212 0.0828 RC _{iii} C4-C3-C2-N1-H14 0.0084 0.2024 RC _{iv} H17-C3-C4-C12-C11-H24 0.0041 0.4058	A_{iii}	C2-H15···H24-C11	-0.0035	0.1512
RC _{iii} C4-C3-C2-N1-H14 0.0084 0.2024 RC _{iv} H17-C3-C4-C12-C11-H24 0.0041 0.4058	RC_i	C4-C5-N6-C7-C12	0.0493	0.0257
RC _{iν} H17-C3-C4-C12-C11-H24 0.0041 0.4058	RC_{ii}	C7-C8-C9-C10-C11-C12	0.0212	0.0828
10	RC_{iii}	C4-C3-C2-N1-H14	0.0084	0.2024
RC H15-C2-C3-C4-C12-C11-H24 0.0035 0.1612	$RC_{i\nu}$	H17-C3-C4-C12-C11-H24	0.0041	0.4058
110 02 00 0, 012 011 112, 0.0000 0.1012	RC_{ν}	H15-C2-C3-C4-C12-C11-H24	0.0035	0.1612

^aThe assignments are based on the topological parameters, including electron densities, $\rho(\mathbf{r})$, and their product with the sign of the λ_2 eigenvalues of the Hessian matrices, $\rho(\mathbf{r})^* = \text{sign}(\lambda_2)\rho(\mathbf{r})$, for the minima of the reduced density gradient, $s(\mathbf{r})$. The notation of the atoms involved in the interactions is shown in Figure 4(a).

interactions. Specifically, the A_i interaction corresponds to the blue isosurface in Figure 4, between the amino hydrogen and the π system of the pyrrole ring, and A_{ii} and A_{iii} C-H···H-C interactions correspond to the green isosurfaces, between two different hydrogens of the ethyl group and the hydrogen pointing toward them on the benzene ring and A_{ii} .

The finding that the weak NH··· π interaction contributes to the stabilization of the TRA Gpy(out) conformer is in line with previous propositions; ^{35,42} however, it appears here that the A_i and A_{iii} C-H···H-C interactions related to hydrogen—hydrogen bonding ^{49,50} also play a role. In these interactions, hydrogen atoms bonded to different carbon atoms tolerate identical or similar electron charges while coming into close contact and slightly stabilizing the molecule. This behavior implies that the topology of the carbon skeleton in the ethylamino chain affects these interactions. Furthermore, despite the weakness of the C-H···H-C and N-H··· π interactions, it seems that their buildup between the ethylamino chain and different portions of the indole results in TRA Gpy(out) conformer stabilization.

It is interesting to compare the attractive interactions observed here to those arising in the most stable *gauche* conformer of 2-(4-fluorophenyl)-ethylamine. He found in the latter, by NCI analysis, that in addition to the N–H··· π interaction, which is somewhat more intense than in the TRA Gpy(out) conformer, the C–H···N (the C–H of the phenyl with the amino N) also fulfills a role but no C–H···H–C interactions. The appearance of C–H···H–C interactions in the TRA conformer is probably due to the larger indole moiety, where the C–H bonds of the chain can come closer to the benzene C–H.

In addition, besides bonding (negative $\rho(\mathbf{r})^*$) interactions, nonbonding (positive) interactions occur due to local depletion of the electron density ($\lambda_2 > 0$). These interactions correspond to ring-critical points positioned in the center of the pyrrole, RC_i, and benzene, RC_{ii}, rings. Also, some additional repulsive interactions, RC_{iii} and RC_v, occur due to five- up to seven-membered ring formations, respectively, incorporating the ethylamino chain atoms. The RC_{iii} interaction represents the ring formed by the C4–C3–C2–N1–H14 atoms, where the last two are involved in the N–H··· π interaction, A_i. These interactions are evident from the blue isosurface, shown in Figure 4(a), which changes color to a mixed color scheme that varies sign, leading to two

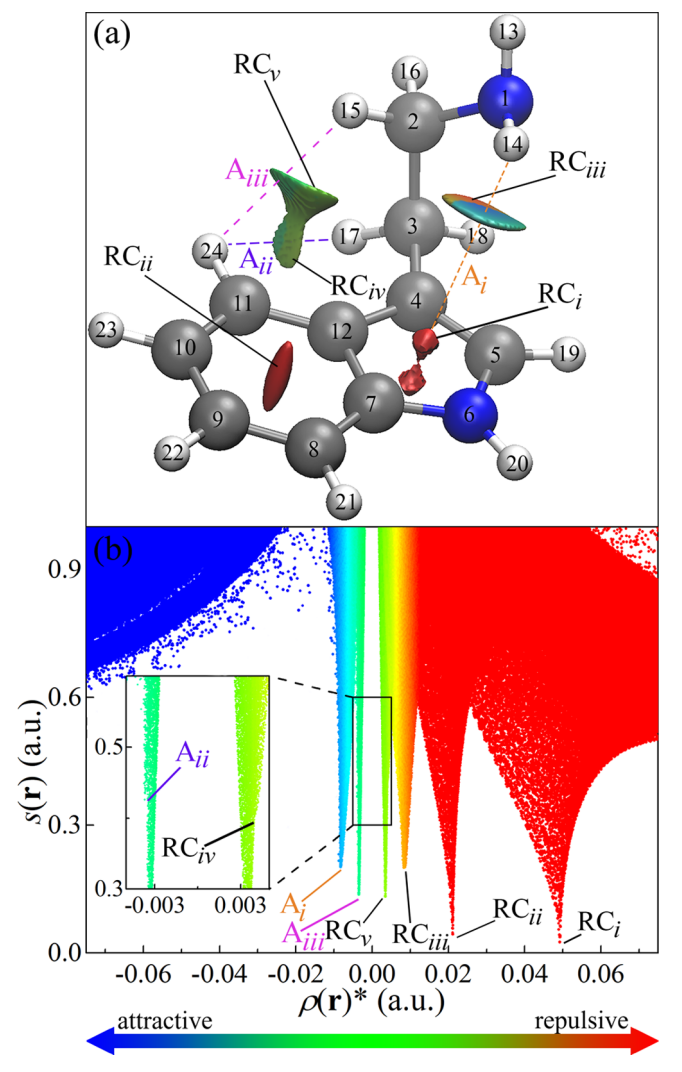


Figure 4. Gpy(out) conformer of tryptamine: (a) isosurfaces of the noncovalent interactions at a reduced density gradient $s(\mathbf{r})=0.6$ (a.u.) with electron density $\rho(\mathbf{r})<0.01$ (a.u.) cutoff and (b) visualization plot of $s(\mathbf{r})$ against the electron densities and the λ_2 eigenvalues of the Hessian matrices $[\rho(\mathbf{r})^* (= \text{sign}(\lambda_2)\rho(\mathbf{r}))$ in a.u.] (bottom), as obtained from the analysis of the optimized structure at the B3LYP/6-311⁺⁺G(d,p) level of theory. The color schemes in (a) and (b) and in the bottom arrows are similar, indicating the type of interactions. In the inset of (b), the expanded visualization plot of the troughs in $s(\mathbf{r})$ appears, showing that A_{ii} and RC_{iv} adjoin A_{iii} and RC_{vv} respectively. The ring closures outlined in Table 1 are denoted by RC.

differentiated parts. The blue part illustrates the directional N–H··· π interaction, and the red part indicates the strain in the five-membered ring, resulting from a multicentric density close to the ethylamino chain. In addition, the RC_{iv} and RC_v intramolecular ring closures, including atoms of the ethylamino tail and relatively close lying phenyl atoms, also increase somewhat the electron density and induce strain in the region of the A_{ii} and A_{iii} isosurfaces, turning them slightly yellow. Consequently, the attractive NCIs play a pivotal role in affecting the TRA Gpy(out) conformer structure, but the repulsive ones are important too, enabling the balancing of both types and dictating the conformer structure.

To summarize, we performed here the first experiment that integrates LDJC and ILSRS, allowing extension of the available frequency range for studying the vibrational signatures of nonvolatile samples. Our focus was on the ILSR vibrational spectrum of the most stable gas-phase TRA conformer, in the high- and low-frequency regions, following its preparation by LDJC. The ILSR spectrum of the TRA Gpy(out) conformer was analyzed with DFT calculations of the characteristic Raman spectrum, identifying the conformational structure. The features appearing in the spectrum were found to match various normal mode vibrations, assessing the electronic structure of the TRA Gpy(out) conformer. The structure of this conformer is characterized by an ethylamino side chain, folded in a gauche configuration, where the amino hydrogen points toward the pyrrole π cloud, and the nitrogen lone pair is oriented away from the indole π cloud. The deduced electronic structure offered the possibility to obtain insight into its structure by NCI analysis, allowing evaluation of the contributing interactions.

By considering the reduced gradient isosurfaces and the visualization plot that provided troughs in the reduced density gradient, obtained by NCI, it was possible to determine the attractive and repulsive interactions. These interactions were classified by considering the λ_2 eigenvalue, which varies its sign depending on attractive (negative) and repulsive (positive) interactions. We found that the structure of this conformer involves attractive weak C-H···H-C interactions and the N- $H \cdots \pi$ hydrogen bond as well as repulsive interactions that form five- to seven-membered rings that encompass the atoms of the ethylamino chain. While the N-H $\cdots\pi$ hydrogen bond was previously suggested to stabilize the structure, 35,42 it appears, based on the NCI analysis, that other C-H···H-C interactions also play a role. Hence, the compromise between the attractive and repulsive interactions is key in exerting the stabilization of the TRA conformer. This unique combination of LDJC and ILSRS, together with quantum calculations, provides access to vibrational signatures of isolated nonvolatile molecules by tabletop laser sources at uniform resolution and in a broad frequency range, expanding the ability to study complex molecules in the gas phase. We believe that this approach opens an additional window toward studying nonvolatile complex molecules and obtaining an in-depth understanding of the various interactions in these systems.

METHODS

TRA is mixed with graphite powder at a 4:1 ratio and pressed into a channel of a translating graphite bar. This mixture is desorbed using a neodymium:yttrium aluminum garnet (Nd:YAG) laser beam (1064 nm, ~8 ns pulsewidth, 10 Hz repetition rate), delivered via several optical components into an optical fiber with numerical apertures of 0.22.31 The end of the optical fiber positioned inside the vacuum chamber is cleaved and positioned in a stainless steel cylinder, just in front of the valve orifice and at \sim 1 mm distance. The laser fluence and the spot size of the desorption beam are controlled by inserting, just before coupling into the optical fiber, two linear polarizers with a half-wave plate and by altering the optical fiber height above the sample, respectively. Laser fluences of $0.4-1 \text{ J/cm}^2$ and spots of $\sim 1 \text{ mm}$ diameter (dia.) are used for LD. The sample movement under the laser beam is at a speed of 0.01 mm/s, and the desorbed material is entrained in a supersonic expansion of argon gas (10 bar backing pressure), delivered by a pulsed valve with a 0.79 mm dia., cone-shaped orifice, polyether ether ketone (PEEK) poppet, and a \sim 120 μ s pulse width for JC. The molecular beam then passes through a 2 mm diameter skimmer, with the apex positioned ~68 mm

downstream of the valve. The R2PI and ILSRS signals, resulting from probing the cold, gaseous molecules, are detected in a home-built time-of-flight mass spectrometer (TOFMS).

One-color R2PI measurements are performed following the skimming of the molecular beam and its entrance into the interaction region, midway between the repeller (R) and extractor (E) electrodes. By using a tunable UV beam [blue beam in Figure 1(a)], obtained from a frequency-doubled pulsed dye laser pumped by a frequency-doubled Nd:YAG laser (5 ns pulses, 10 Hz repetition rate, $\sim\!10~\mu\mathrm{J}$ per pulse, and $\sim\!0.5~\mathrm{J/cm^2}$ fluence) the mass-selected R2PI spectrum of TRA is measured while scanning across the origin of the $S_1 \leftarrow S_0$ electronic transitions of the TRA conformers.

The VIS beams for ILSRS, Figure 1(b), are generated by an additional frequency doubled Nd:YAG laser (532 nm, ~5 ns pulses at 10 Hz) [green beam in Figure 1(a)]. This secondharmonic laser beam is divided in a 1:7 ratio, where the weaker beam served as $\omega_{\rm p}$ and the stronger one pumps a dye laser and provides the ω_S [red beam in Figure 1(a)]. The counterpropagating vertically polarized ω_{p} (entered from the same side of the chamber as the UV beam) and $\omega_{\rm S}$ beams with energies of ~20 and ~25 mJ per pulse, following focusing by 35 and 30 cm focal length (f.l.) planoconvex lenses, are spatially and temporally overlapped in the interaction region of the TOFMS. The VIS beams precede the ionization pulse by \sim 26 ns, and the ω_s beam is scanned across selected wavelength regions while tuning and parking the UV pulse on the R2PI transition of the most stable TRA conformer. The ensuing ions are detected by a microchannel plate while feeding the resulting signal through a homemade fast preamplifier into a fast digital oscilloscope. This procedure allows measurement of mass spectra or integrated intensities of the TRA ion peak at mass channel m/z = 160.

The equilibrium structure of the dominant conformer of TRA is obtained by initially optimizing the molecule with the Merck molecular force field (MMFF94s) in the Avogadro molecular editor and visualization tool.⁵¹ Then, this geometry is further optimized, with Gaussian 09,52 using DFT calculations with the Becke three-parameter hybrid functional combined with the Lee–Yang–Parr correlation functional $(B3LYP)^{53,54}$ and the 6-311⁺⁺G(d,p) basis set to obtain the energetic, structural, vibrational, and electronic properties of TRA. The harmonic frequencies of vibrations are scaled by the previously derived factors²³ of 0.956 and 0.964 for the N-H and C-H stretches, respectively, and 0.946 for the low <1600 cm⁻¹ frequency range. Finally, the calculated Raman spectra are obtained while accounting for the Raman activities, converted to Raman intensities, 42 and, for the scaled harmonic fundamental frequencies, convolved with pure Lorentzian lines of fwhm of 0.5 cm⁻¹. The assignment of the probed conformer and the involved vibrational modes is obtained by finding the calculated features that best match the measured ones. We generated visualization of the structure and the displacement vectors, corresponding to the identified vibrational modes, by Gauss View. 46 The calculated structure is also used for assessing the NCIs in TRA and for illustrating the interactions by the NCIPLOT⁴⁴,⁴⁵ while evaluating the electron density regions in which the reduced density gradient diminished and providing iso-surfaces of the gradient.

AUTHOR INFORMATION

Corresponding Author

Ilana Bar – Department of Physics, Ben-Gurion University of the Negev, Beer-Sheva 8410501, Israel; orcid.org/0000-0002-4032-1904; Email: ibar@bgu.ac.il

Authors

Afik Shachar – Department of Physics, Ben-Gurion University of the Negev, Beer-Sheva 8410501, Israel

Itai Kallos — Department of Physics, Ben-Gurion University of the Negev, Beer-Sheva 8410501, Israel

Mattanjah S. de Vries – Department of Chemistry & Biochemistry, University of California Santa Barbara, Santa Barbara, California 93106, United States; orcid.org/0000-0001-5007-8074

Complete contact information is available at: https://pubs.acs.org/10.1021/acs.jpclett.1c03336

Author Contributions

§A.S. and I.K. contributed equally.

Notes

The authors declare no competing financial interest.

■ ACKNOWLEDGMENTS

We would like to acknowledge the financial support of this research by the United States—Israel Binational Science Foundation (BSF) under Grant 2014370 and the Israel Science Foundation (ISF) founded by the Israel Academy of Sciences and Humanities, Grant 519/15. This work was also supported by the National Science Foundation under CHE-1800283.

REFERENCES

- (1) Bakels, S.; Gaigeot, M.-P.; Rijs, A. M. Gas-Phase Infrared Spectroscopy of Neutral Peptides: Insights from the Far-IR and THz Domain. *Chem. Rev.* **2020**, *120*, 3233–3260.
- (2) Schwing, K.; Gerhards, M. Investigations on Isolated Peptides by Combined IR/UV Spectroscopy in a Molecular Beam–Structure, Aggregation, Solvation and Molecular Recognition. *Int. Rev. Phys. Chem.* **2016**, *35*, 569–677.
- (3) Rijs, A. M.; Oomens, J. IR Spectroscopic Techniques to Study Isolated Biomolecules. *Top. Curr. Chem.* **2014**, 364, 1–42.
- (4) Gloaguen, E.; Mons, M. Isolated Neutral Peptides. Top. Curr. Chem. 2014, 364, 225-270.
- (5) de Vries, M. S. Gas-Phase IR Spectroscopy of Nucleobases. *Top. Curr. Chem.* **2014**, 364, 271–297.
- (6) Cocinero, E. J.; Çarçabal, P. Carbohydrates. *Top. Curr. Chem.* **2014**, 364, 299–333.
- (7) Kleinermanns, K.; Nachtigallová, D.; de Vries, M. S. Excited State Dynamics of DNA Bases. *Int. Rev. Phys. Chem.* **2013**, 32, 308–342
- (8) Zwier, T. S. Laser Probes of Conformational Isomerization in Flexible Molecules and Complexes. *J. Phys. Chem. A* **2006**, *110*, 4133–4150.
- (9) de Vries, M. S.; Hobza, P. Gas-Phase Spectroscopy of Biomolecular Building Blocks. *Annu. Rev. Phys. Chem.* **2007**, *58*, 585–612.
- (10) Robertson, E. G.; Simons, J. P. Getting into Shape: Conformational and Supramolecular Landscapes in Small Biomolecules and their Hydrated Clusters. *Phys. Chem. Chem. Phys.* **2001**, 3, 1–18.
- (11) Berden, G.; Meerts, W. L.; Kreiner, W. High-Resolution Laser-Induced Fluorescence and Microwave-Ultraviolet Double Resonance Spectroscopy on 1-cyanonaphthalene. *Chem. Phys.* **1993**, *174*, 247–253.

- (12) Page, R. H.; Shen, Y. R.; Lee, Y. T. Local Modes of Benzene and Benzene Dimer, Studied by Infrared–Ultraviolet Double Resonance in a Supersonic Beam. *J. Chem. Phys.* **1988**, *88*, 4621–4636.
- (13) Tanabe, S.; Ebata, T.; Fujii, M.; Mikami, N. OH Stretching Vibrations of Phenol- $(H2O)_n$ (n=1-3) Complexes Observed by IR-UV Double-Resonance Spectroscopy. *Chem. Phys. Lett.* **1993**, 215, 347–352.
- (14) Yamamoto, R.; Ebata, T.; Mikami, N. Stimulated Raman Spectroscopic Study on Intermolecular Vibrations of Size-Selected Benzonitrile Clusters. *Eur. Phys. J. D* **2002**, *20*, 403–408.
- (15) Golan, A.; Mayorkas, N.; Rosenwaks, S.; Bar, I. Raman Spectral Signatures as Conformational Probes of Gas Phase Flexible Molecules. *J. Chem. Phys.* **2009**, *131*, 024305.
- (16) Saigusa, H.; Lim, E. C. Pump-Probe Fluorescence Studies of Excimer Formation and Dissociation for the Van Der Waals Dimer of Fluorene. *J. Phys. Chem.* **1991**, 95, 2364–2370.
- (17) Dagdigian, P. J.; Zare, R. N. tunable Laser Fluorescence Method for Product State Analysis. *Science* **1974**, *185*, 739–747.
- (18) Feldman, D. L.; Lengel, R. K.; Zare, R. N. Multiphoton Ionization: A Method for Characterizing Molecular Beams and Beam Reaction Products. *Chem. Phys. Lett.* **1977**, *52*, 413–417.
- (19) Boesl, U.; Neusser, H. J.; Schlag, E. W. Two-Photon Ionization of Polyatomic Molecules in a Mass Spectrometer. *Z. Naturforsch., A: Phys. Sci.* **1978**, *33a*, 1546–1548.
- (20) Lipert, R. J.; Colson, S. D. Persistent Spectral Hole Burning of Molecular Clusters in a Supersonic Jet. *J. Phys. Chem.* **1989**, *93*, 3894–3896.
- (21) Mayorkas, N.; Malka, I.; Bar, I. Ionization-Loss Stimulated Raman Spectroscopy for Conformational Probing of Flexible Molecules. *Phys. Chem. Chem. Phys.* **2011**, *13*, 6808–6815.
- (22) Mayorkas, N.; Cohen, S.; Sachs, H.; Bar, I. Photofragment Ionization-Loss Stimulated Raman Spectroscopy of a Hydrated Neurotransmitter: 2-Phenylethylamine—Water. RSC Adv. 2014, 4, 58752—58757.
- (23) Mayorkas, N.; Sachs, H.; Schütz, M.; Ishiuchi, S.-I.; Fujii, M.; Dopfer, O.; Bar, I. Structural Motifs of 2-(2-Fluoro-phenyl)-Ethylamine Conformers. *Phys. Chem. Chem. Phys.* **2016**, *18*, 1191–1201.
- (24) Shachar, A.; Mayorkas, N.; Bar, I. Structural Features of Monohydrated 2-(4-Fluorophenyl) Ethylamine: A Combined Spectroscopic and Computational Study. *Phys. Chem. Chem. Phys.* **2017**, 19, 23999–24008.
- (25) Bernhard, D.; Fatima, M.; Poblotzki, A.; Steber, A. L.; Perez, C.; Suhm, M. A.; Schnell, M.; Gerhards, M. Dispersion-Controlled Docking Preference: Multi-Spectroscopic Study on Complexes of Dibenzofuran with Alcohols and Water. *Phys. Chem. Chem. Phys.* **2019**, 21, 16032–16046.
- (26) Bakker, D. J.; Dey, A.; Tabor, D. P.; Ong, Q.; Mahé, J.; Gaigeot, M. P.; Sibert, E. L., III; Rijs, A. M. Fingerprints of Inter- and Intramolecular Hydrogen Bonding in Saligenin-Water Clusters Revealed by Mid- and Far-Infrared Spectroscopy. *Phys. Chem. Chem. Phys.* **2017**, *19*, 20343–20356.
- (27) Levis, R. J. Laser Desorption and Ejection of Biomolecules from the Condensed Phase into the Gas Phase. *Annu. Rev. Phys. Chem.* **1994**, *45*, 483–518.
- (28) Meijer, G.; de Vries, M. S.; Hunziker, H. E.; Wendt, H. R. Laser Desorption Jet-Cooling of Organic Molecules. *Appl. Phys. B: Lasers Opt.* **1990**, *51*, 395–403.
- (29) Piuzzi, F.; Dimicoli, I.; Mons, M.; Tardivel, B.; Zhao, Q. A Simple Laser Vaporization Source for Thermally Fragile Molecules Coupled to a Supersonic Expansion: Application to the Spectroscopy of Tryptophan. *Chem. Phys. Lett.* **2000**, 320, 282–288.
- (30) Mayorkas, N.; Rudić, S.; Davis, B. G.; Simons, J. P. Heavy Water Hydration of Mannose: The Anomeric Effect in Solvation, Laid Bare. *Chem. Sci.* **2011**, *2*, 1128–1134.
- (31) Shachar, A.; Kallos, I.; de Vries, M. S.; Bar, I. A Compact and Cost-Effective Laser Desorption Source for Molecular Beam

- Generation: Comparison with Simulations. J. Phys. B: At., Mol. Opt. Phys. 2021, 54, 175401.
- (32) Park, Y. D.; Rizzo, T. R.; Peteanu, L. A.; Levy, D. H. Electronic Spectroscopy of Tryptophan Analogs in Supersonic Jets: 3-Indole Acetic Acid, 3-Indole Propionic Acid, Tryptamine, and N-Acetyl Tryptophan Ethyl Ester. J. Chem. Phys. 1986, 84, 6539-6549.
- (33) Philips, L. A.; Levy, D. H. Determination of the Transition Moment and the Geometry of Tryptamine by Rotationally Resolved Electronic Spectroscopy. J. Phys. Chem. 1986, 90, 4921-4923.
- (34) Philips, L. A.; Levy, D. H. Rotationally Resolved Electronic Spectroscopy of Tryptamine Conformers in a Supersonic Jet. J. Chem. Phys. 1988, 89, 85-90.
- (35) Carney, J. R.; Zwier, T. S. The Infrared and Ultraviolet Spectra of Individual Conformational Isomers of Biomolecules: Tryptamine. J. Phys. Chem. A 2000, 104, 8677-8688.
- (36) Nguyen, T.; Pratt, D. W. Permanent Electric Dipole Moments of Four Tryptamine Conformers in the Gas Phase: A New Diagnostic of Structure and Dynamics. J. Chem. Phys. 2006, 124, 054317.
- (37) Pei, L.; Zhang, J.; Wu, C.; Kong, W. Conformational Identification of Tryptamine Embedded in Superfluid Helium Droplets using Electronic Polarization Spectroscopy. J. Chem. Phys. 2006, 125, 024305.
- (38) Schmitt, M.; Feng, K.; Böhm, M.; Kleinermanns, K. Low Frequency Backbone Vibrations of Individual Conformational Isomers: Tryptamine. J. Chem. Phys. 2006, 125, 144303.
- (39) Gu, Q.; Knee, J. L. Zero Kinetic Energy Photoelectron Spectroscopy of Tryptamine and the Dissociation Pathway of the Singly Hydrated Cation Cluster. J. Chem. Phys. 2012, 137, 104312.
- (40) Sakota, K.; Kouno, Y.; Harada, S.; Miyazaki, M.; Fujii, M.; Sekiya, H. IR Spectroscopy of Monohydrated Tryptamine Cation: Rearrangement of the Intermolecular Hydrogen Bond induced by Photoionization. J. Chem. Phys. 2012, 137, 224311.
- (41) Mayorkas, N.; Izbitski, S.; Bernat, A.; Bar, I. Simultaneous Ionization-Detected Stimulated Raman and Visible-Visible-Ultraviolet Hole-Burning Spectra of Two Tryptamine Conformers. J. Phys. Chem. Lett. 2012, 3, 603-607.
- (42) Mayorkas, N.; Bernat, A.; Izbitski, S.; Bar, I. Vibrational and Vibronic Spectra of Tryptamine Conformers. J. Chem. Phys. 2013, 138, 124312.
- (43) Schmitt, M.; Spiering, F.; Zhaunerchyk, V.; Jongma, R. T.; Jaeqx, S.; Rijs, A. M.; van der Zande, W. J. Far-Infrared Spectra of the Tryptamine A Conformer by IR-UV Ion Gain Spectroscopy. Phys. Chem. Chem. Phys. 2016, 18, 32116-32124.
- (44) Johnson, E. R.; Keinan, S.; Mori-Sánchez, P.; Contreras-García, J.; Cohen, A. J.; Yang, W. Revealing Noncovalent Interactions. J. Am. Chem. Soc. 2010, 132, 6498-6506.
- (45) Contreras-Garcia, J.; Johnson, E. R.; Keinan, S.; Chaudret, R.; Piquemal, J. P.; Beratan, D. N.; Yang, W. NCIPLOT: A Program for Plotting Noncovalent Interaction Regions. J. Chem. Theory Comput. 2011, 7, 625-632.
- (46) Dennington, II, R.; Keith, T.; Millam, J.; Eppinnett, K.; Hovell, W. L.; Gilliland, R. GaussView, Version 3.09; Semichem Inc.: Shawnee Mission, KS, 2003.
- (47) Chaudret, R.; de Courcy, B.; Contreras-García, J.; Gloaguen, E.; Zehnacker-Rentien, A.; Mons, M.; Piquemal, J.-P. Unraveling Non-Covalent Interactions within Flexible Biomolecules: From Electron Density Topology to Gas Phase Spectroscopy. Phys. Chem. Chem. Phys. 2014, 16, 9876-9891.
- (48) Laplaza, R.; Peccati, F.; Boto, R. A.; Quan, C.; Carbone, A.; Piquemal, J.-P.; Maday, Y.; Contreras-García, J. NCIPLOT and the Analysis of Noncovalent Interactions using the Reduced Density Gradient. Wiley Interdiscip. Rev.: Comput. Mol. Sci. 2021, 11, No. e1497.
- (49) Matta, C. F.; Hernández-Trujillo, J.; Tang, T.-H.; Bader, R. F. W. Hydrogen-Hydrogen Bonding: A Stabilizing Interaction in Molecules and Crystals. Chem. - Eur. J. 2003, 9, 1940-1951.
- (50) Matczak, P. Intramolecular C-H··· H-C Contacts in Diheteroaryl Ketones and Thioketones: A Theoretical Analysis. Bull. Chem. Soc. Jpn. 2016, 89, 92-102.

- (51) Hanwell, M. D.; Curtis, D. E.; Lonie, D. C.; Vandermeersch, T.; Zurek, E.; Hutchison, G. R. J. Avogadro: An Advanced Semantic Chemical Editor, Visualization, and Analysis Platform. J. Cheminf. 2012, 4, 17.
- (52) Frisch, M. J.; Trucks, G. W.; Schlegel, H. B.; Scuseria, G. E.; Robb, M. A.; Cheeseman, J. R.; Scalmani, G.; Barone, V.; Mennucci, B.; Petersson, G. A.; Nakatsuji, H.; Caricato, M.; Li, X.; Hratchian, H. P.; Izmaylov, A. F.; Bloino, J.; Zheng, G.; Sonnenberg, J. L.; Hada, M.; Ehara, M.; Toyota, K.; Fukuda, R.; Hasegawa, J.; Ishida, M.; Nakajima, T.; Honda, Y.; Kitao, O.; Nakai, H.; Vreven, T.; Montgomery, J. A., Jr.; Peralta, J. E.; Ogliaro, F.; Bearpark, M.; Heyd, J. J.; Brothers, E.; Kudin, K. N.; Staroverov, V. N.; Kobayashi, R.; Normand, J.; Raghavachari, K.; Rendell, A.; Burant, J. C.; Iyengar, S. S.; Tomasi, J.; Cossi, M.; Rega, N.; Millam, J. M.; Klene, M.; Knox, J. E.; Cross, J. B.; Bakken, V.; Adamo, C.; Jaramillo, J.; Gomperts. R.; Stratmann, R. E.; Yazyev, O.; Austin, A. J.; Cammi, R.; Pomelli, C.; Ochterski, J. W.; Martin, R. L.; Morokuma, K.; Zakrzewski, V. G.; Voth, G. A.; Salvador, P.; Dannenberg, J. J.; Dapprich, S.; Daniels, A. D.; Farkas, O.; Foresman, J. B.; Ortiz, J. V.; Cioslowski, J.; Fox, D. J. Gaussian 09, revision C.01; Gaussian, Inc.: Wallingford, CT, 2009.
- (53) Becke, A. D. Density-Functional Exchange-Energy Approximation with Correct Asymptotic Behavior. Phys. Rev. A: At., Mol., Opt. Phys. 1988, 38, 3098-3100.
- (54) Lee, C.; Yang, W.; Parr, R. G. Development of the Colle-Salvetti Correlation-Energy Formula into A Functional of the Electron Density. Phys. Rev. B: Condens. Matter Mater. Phys. 1988, 37, 785-

NOTE ADDED AFTER ASAP PUBLICATION

This paper was published ASAP on November 12, 2021, with errors in Figure 1. The corrected version was reposted November 15, 2021.